Pullout Capacity of Headed Anchors in Prestressed Concrete

R. Piccinin, Ph.D.[1]; R. Ballarini, Ph.D., F.ASCE[2]; and S. Cattaneo, Ph.D.[3]

Abstract: A combined experimental and computational study shows that the pullout capacity of anchors embedded at small depths in prestressed concrete is associated with the strongest possible (linear elastic fracture mechanics) size effect. A design formula is proposed that reflects the effects of embedment depth and the nondimensional parameters that quantify the level of prestressing and the characteristic length of the matrix. **DOI: 10.1061/(ASCE)EM.1943-7889.0000395.**

CE Database subject headings: Anchors; Finite element method; Prestressed Concrete; Cracking; Axisymmetry; Pullout.

Author keywords: Anchors; Concrete breakout; Finite-element method; Cohesive elements; Axisymmetry; Prestressed concrete; Cracking.

Introduction

Headed anchors are structural steel elements used to connect and, thus, transfer forces from one concrete component to another. Among the several types of failure, the one occurring as a result of the anchors pulling out of the concrete matrix has been the most widely investigated and represents the biggest concern for structural engineering applications. In the mid-1980s, formulas for the prediction of load-carrying capacity in the case of concrete pullout relied on plasticity-based models, which assumed a constant tensile stress acting on the projected area of a conical failure surface oriented at 45° with respect to the plane of the anchor head (Jensen and Braestrup 1976; ACI 1989).

Experimental and analytical investigations (Ottosen 1981; Ballarini et al. 1986, 1987; Eligehausen and Sawade 1989; Eligehausen and Ozbolt 1990; Ozbolt et al. 1999) demonstrated that formulas based on plasticity were incorrect and unconservative for typical anchor embedment depths and that experimentally measured load-carrying capacity could be accurately predicted using fracture mechanics models. The fracture mechanics paradigm is a result of recognition that the failure of headed anchors reflects the progressive propagation of discrete cracks. The resulting linear elastic fracture mechanics (LEFM)-based concrete capacity design (CCD) formula (Fuchs et al. 1995) can be expressed as

$$P_u \approx K_c \cdot d^{3/2} \approx k_{nc} \cdot \sqrt{f'_c} \cdot d^{3/2} \tag{1}$$

where P_u, K_c, f'_c, d, and k_{nc} = load-carrying capacity, fracture toughness, compressive strength, embedment depth, and the empirical constant relating toughness to compressive strength, respectively. Eq. (1) was adopted by several international building codes, such as ACI 318 (ACI 2008), ACI 349 (ACI 2006), and the Comité Euro-International du Béton design (CEB 1997), and was calibrated through numerous experimental programs and expresses the correct dependence of the ultimate pullout capacity of headed anchors on embedment depth. Additional and important studies were completed by Ozbolt et al. (1999). In their investigations, experimental and numerical results confirmed the strong size effect on the concrete pullout failure strength for a broad range of embedment depths larger than 1.5 in. (about 40 mm). Despite the large number of data, no investigations were conducted on the behavior of very shallow anchors (i.e., embedment $d < 1.5$ in.).

According to ACI 318 Appendix D (ACI 2008), the CCD formula can be used to predict the 5% fractile of the concrete breakout loads only for situations in which the concrete matrix is uncracked (unstressed) and for anchors with a relatively small head (mean bearing pressure at maximum load of approximately $13f'_c$). When cracking as a result of external loads (e.g., tension zones, negative moment loading conditions) or imposed deformations (e.g., creep, shrinkage, temperature) is expected in the region in which the anchor is placed, a 25% reduction in pullout capacity is prescribed. This is achieved by reducing the constant k_{nc} in Eq. (1).

Modifications to the CCD formula for anchors placed in compressively prestressed concrete have not been contemplated and have received less attention. Within the context of plasticity theory, three-dimensional (3D) constitutive models for concrete subjected to a triaxial state of stress were used for structural analyses of headed and undercut anchors (Pivonka et al. 2004). Baran et al. (2006) performed experiments on various types of cast-in-place inserts to determine the influence of reinforcement and prestress. As expected, they observed that the presence of a prestressing force in the direction orthogonal to the axes of the inserts embedded in reinforced concrete resulted in an increase in load capacity and ductility. Despite this unique experimental investigation, no formulas or recommendations and, above all, no insights on the fundamental mechanics of the problem were proposed. By following Ballarini et al. (1986, 1987) and Vogel and Ballarini (1999), Piccinin et al. (2010) investigated the effects of compressive and tensile fields on the capacity of headed anchors using LEFM. Preliminary experimental results showed that for embedments that are not too shallow, the model correctly predicts a linear

[1]Technical Service Engineer, Hilti, Inc., 5400 South 122nd East Ave., Tulsa, OK 74146 (corresponding author). E-mail: picci007@umn.edu

[2]James L. Record Professor and Head, Dept. of Civil Engineering, Univ. of Minnesota, SE 500 Pillsbury Dr., Minneapolis, MN 55455-0116. E-mail: broberto@umn.edu

[3]Associate Professor, Dept. of Structural Engineering, Politecnico di Milano, Milan, Italy. E-mail: cattaneo@stru.polimi.it

Note. This manuscript was submitted on June 26, 2011; approved on December 19, 2011; published online on December 23, 2011. Discussion period open until December 1, 2012; separate discussions must be submitted for individual papers. This paper is part of the ***Journal of Engineering Mechanics***, Vol. 138, No. 7, July 1, 2012. ©ASCE, ISSN 0733-9399/2012/7-877–887/$25.00.

dependence of the pullout force on the compressive stresses applied biaxially to the embedding concrete matrix, and a tentative design formula was proposed. However, for embedment depths of less than 1 in., LEFM could not reproduce the experimentally measured capacity. It was speculated that such shallow embedments may be associated with a relatively large process zone, within which microcracking and aggregate interlock occur. If this is the case, the experimental results reflect a transition from the strongest size effect possible (the inverse square root dependence of nominal strength on size determined by LEFM) to the size-independent behavior demanded by plasticity-based models. Another explanation of the discrepancy between LEFM predictions and experimental data is that the very shallow embedment dimension is comparable to the maximum aggregate size, rendering a highly heterogeneous material that cannot be modeled by a homogeneous continuum.

The work presented in this paper was performed to determine the answer to the previously raised question and develop a design formula that generalizes the CCD formula to cases involving a prestressed matrix. Specifically, the LEFM finite-element model introduced by Vogel and Ballarini (1999) and Piccinin et al. (2010) is generalized to include a cohesive zone that mimics the localized process zone that can develop ahead of a crack front in concrete. The predictions of the model are compared with new experimental results that cover a wider range of embedment depth and fracture energy and that corroborate those obtained in the preliminary experimental program.

LEFM Model and Nondimensional Parameters

Fracture mechanics involves parameter β introduced by Cherepanov (1979)

$$\beta \equiv \frac{L}{r_p} \approx \frac{f_t^2 \cdot L}{K_c^2} \tag{2}$$

where r_p = extent of the process zone that would develop in the vicinity of a very long crack and L = characteristic dimension of the structure. It is noted that β is referred to by the concrete fracture mechanics community as the brittleness number (Bažant and Planas 1998). The value of the brittleness assigned to a specimen configuration through the use of a particular structural dimension in Eq. (2) may not be representative of the brittleness of a different configuration comprised of the same material. For example, the approximate constraint $\beta \geq 2.5$ is suggested for valid toughness testing on beamlike specimens, where the characteristic dimension L is equal to the beam depth. For embedded anchors, the characteristic dimension can be assumed to be equal to the embedment depth, which is typically much smaller than the depth of a beam. Thus, it is not uncommon to find values of $\beta < 1$ (Elfgren and Ohlsson 1992).

Fig. 1(a) shows the maximum nominal stress, $\sigma_N^{\max}$, of a concrete component and illustrates that the brittleness number determines whether failure is of the strength-limited ductile type, or of the toughness-limited brittle type. Noting that L is proportional to d and that any choice of nominal area scales as d^2, plasticity predicts a size-independent strength, whereas LEFM predicts a $1/\sqrt{\beta}$ dependence of strength.

From a design point of view, investigations carried out by Ozbolt et al. (1999) showed that the CCD [Eq. (1)] exhibits a good agreement with the experimental results for the whole size range investigated ($d \geq 1.5$ in.). As shown in Fig. 1(b), where the nominal strength is calculated as the ultimate pullout load divided by the area of a circle with a radius equal to the embedment depth, d, the experimental results show that the size effect on the nominal pullout strength is the strongest possible (Reinhardt 1981; Bažant and Sener 1988). Fig. 1(b) suggests that for embedded anchors there is no transition between the plasticity and the LEFM bounds and that LEFM suffices to predict the load-carrying capacity for all values of embedment. Whether LEFM can be applied to very shallow depths ($d < 1.5$ in.) is yet to be determined.

Fig. 2 shows the cross section of the axisymmetric configuration considered in this study. The headed anchor, embedded at a depth d within a matrix stressed to a level, σ, is represented—as was done by Ballarini et al. (1986, 1987), Vogel and Ballarini (1999), and Piccinin et al. (2010)—by a discontinuity of diameter c with a rigid top surface and a traction-free lower surface. The stem is not considered. The pullout load, P, is represented by the resultant reactive force on the top surface of the discontinuity produced by a uniform stress, p, applied along the bottom surface of the cylindrical model. The curvilinear distance of the traction-free propagating

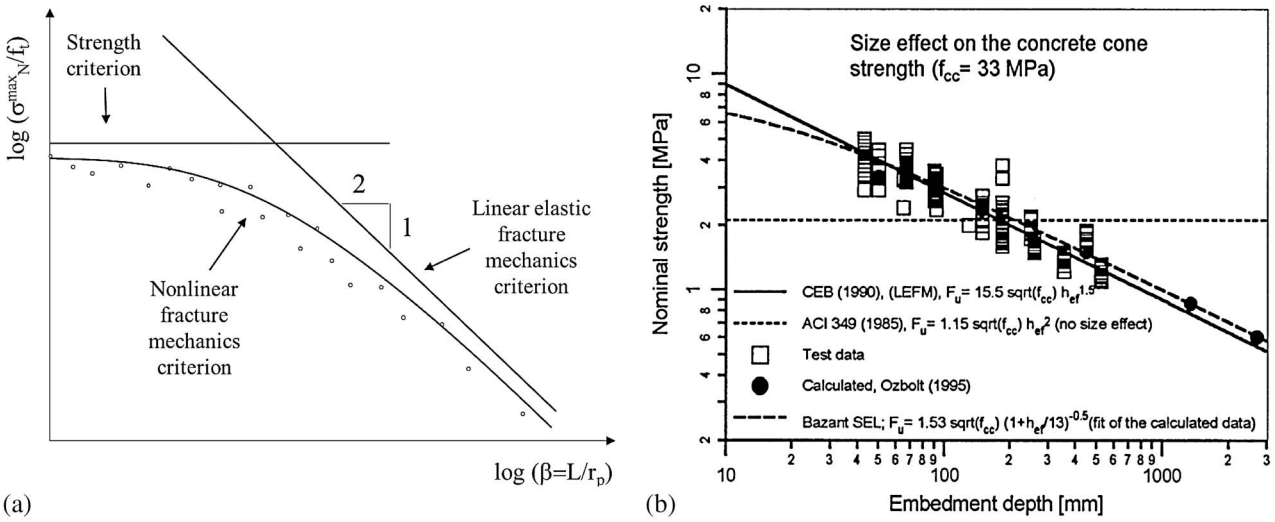

Fig. 1. (a) Normalized nominal strength versus brittleness number; (b) nominal pullout strength as a function of the embedment depth including test data, calculated data, and the size and no size effect prediction formulas (Ozbolt et al. 1999, with permission from the University of Stuttgart)

J. Eng. Mech. 2012.138:877-887.

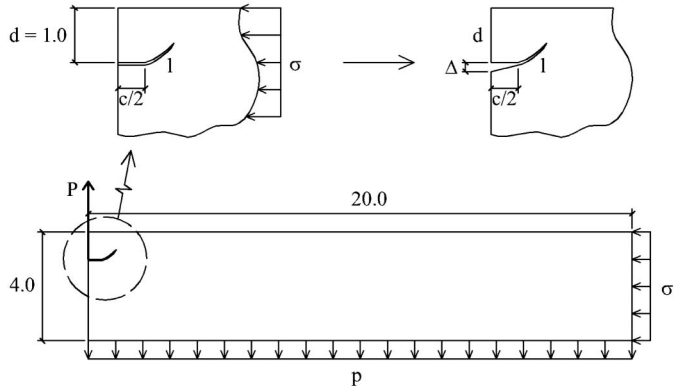

Fig. 2. Cross section of the axisymmetric model of a headed anchor in a prestressed matrix; the axis of rotation/symmetry is represented by the left edge of the section (units in inches)

crack front from the edge of the anchor is defined by l, and the normalized level of stress is defined as $\lambda = \sigma/f_t$ (note that for the compressive case $\lambda > 0$, whereas for the tension case $\lambda < 0$). FRANC2D (Cornell Fracture Group 1997), a program that possesses automatic remeshing capabilities, was used to calculate the stress intensity factors and crack extension direction of the propagating front. More details pertaining to the model can be found in Piccinin (2011).

In the LEFM simulations, by using linearity and dimensional consistency, the ultimate load-carrying capacities were obtained as

$$P_{u,\mathrm{LEFM}} = \max\left[f_1\left(\frac{l}{d},\frac{d}{c},\nu\right)\cdot K_{Ic}\cdot d^{1.5} + f_2\left(\frac{l}{d},\frac{d}{c},\nu\right)\cdot\sigma\right] \quad (3)$$

In terms of β and λ

$$\frac{P_{u,\mathrm{LEFM}}}{f_t\cdot d^2} = \max\left[f_1\left(\frac{l}{d},\frac{d}{c},\nu\right)\cdot\frac{1}{\sqrt{\beta}} + f_2\left(\frac{l}{d},\frac{d}{c},\nu\right)\cdot\lambda\right] \quad (4)$$

Nonlinear Fracture Mechanics Model

The LEFM model was extended to account for the process zone by using zero thickness cohesive elements along the crack faces following Ingraffea and Saouma (1984), Wawrzynek and Ingraffea (1987), and Hellier et al. (1987).

Two methods can be used to model a cohesive crack that is propagating along a curved path. The first method is quick but imprecise, and assumes that the path is not significantly different from what the crack would choose in the absence of the cohesive zone. The procedure involves predicting the path that the crack would follow in the absence of the cohesive zone according to the local symmetry condition (for example, maximum hoop stress, zero local mode-II stress intensity factor, maximum energy release rate conditions) and then calculating the load required to extend the crack along the predicted path when in the presence of the cohesive zone. The second method involves the construction of the crack path through an incremental procedure that searches, at each step, the direction ahead of the front that is perpendicular to the maximum hoop stress. Note that in the first approach the direction is dictated by the stress intensity factors, whereas the second approach is associated with finite stresses along the crack front. Examples of this technique can be found in Bittencourt et al. (1992), Xie and Gerstle (1995), and Ingraffea et al. (1989). The results presented subsequently are for predefined crack paths because it was discovered that the differences in the paths predicted by the two procedures were small compared with the variation in paths observed in the experiments. The details of this investigation can be found in Piccinin (2011).

The crack paths predicted by the maximum hoop stress criterion are shown in Figs. 3 and 4 for selected values of embedment depth, brittleness number, and level of prestress. As expected, and rationalized in Piccinin et al. (2010), the crack path becomes increasingly less steep with increasing level of prestress.

Experimental Program

The experimental program was divided in two parts. In the first part, the experiments documented in Piccinin et al. (2010) were completed. The second part involved concrete with a cylindrical strength of 3.36 ksi (23.17 MPa) and a cubic strength of 4.05 ksi (27.91 MPa). The mix components of the material were portland cement CEM I 52.5 R, according to the ENV 197/1 European Standard, and a natural river aggregate (maximum size of 25 mm). No super plasticizers were added. The concrete had an aggregate/cement ratio of 6.24 and a water/cement ratio of 0.7. The compressive strength of the mix was obtained from compression tests performed on cubes with a 5.9 in. (150 mm) side. The compression tests were completed between 28 and 35 days after the specimens were cast. The concrete properties were recorded and

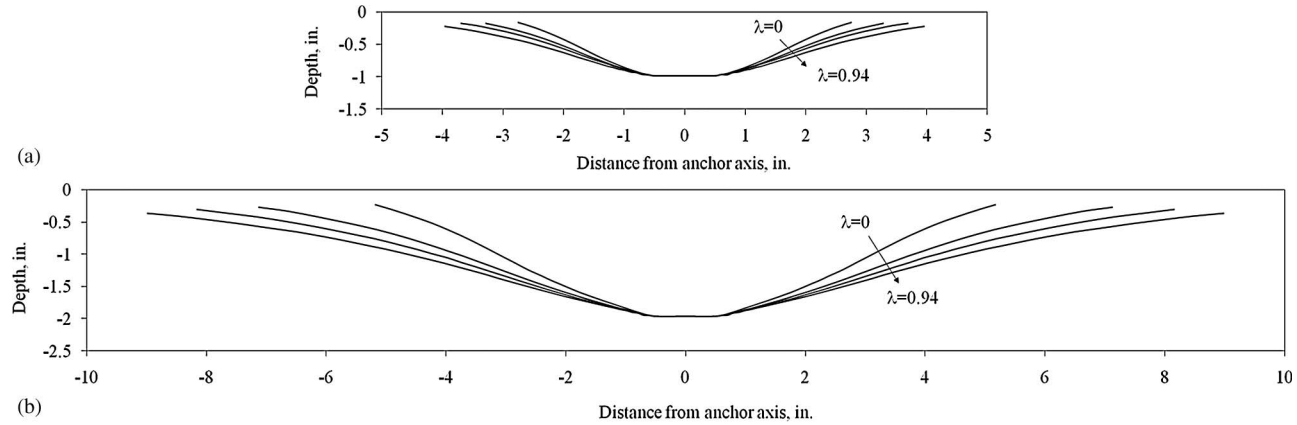

Fig. 3. LEFM crack profiles used for the NLFM simulations: (a) $d/c = 1$ and $\beta = 0.3$; (b) $d/c = 2$ and $\beta = 0.6$

J. Eng. Mech. 2012.138:877-887.

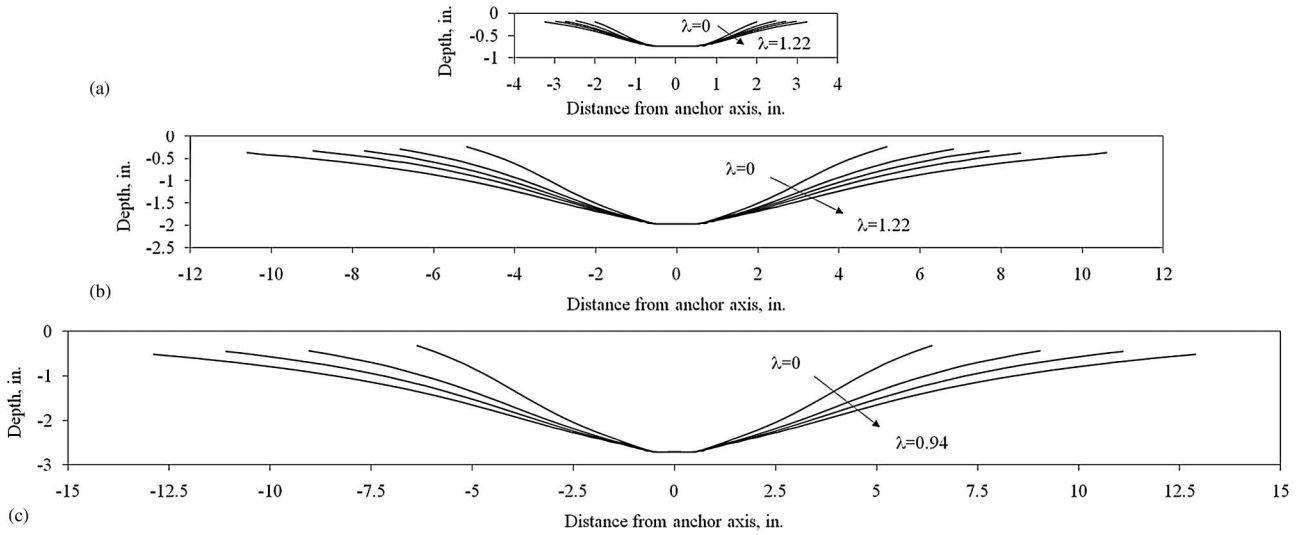

Fig. 4. LEFM crack profiles used for the NLFM simulations: (a) $d/c = 0.75$ and $\beta = 0.31$; (b) $d/c = 2$ and $\beta = 0.82$; (c) $d/c = 2.75$ and $\beta = 1.13$

then averaged. Standard-size cylinders were tested to obtain the indirect tensile strength (splitting test). After averaging, a value of 412 psi was obtained for the concrete indirect tensile strength. The Young's modulus was obtained from available standard design formulas as $E = 57{,}000\sqrt{f'_c}$ psi. The mixture design and the averaged concrete properties for the two parts of the experiments at the time of the tests are reported in Table 1.

All the specimens consisted of concrete blocks with the following dimensions: $39.37 \times 39.37 \times 7.87$ in. ($1 \times 1 \times 0.2$ m). To allow the application of large confining pressures, these dimensions were kept constant and independent of the embedment depth. Four hooks were positioned at the corners to allow for specimen handling.

The concrete anchors had a stem diameter of 0.5 in. (12.7 mm), a head diameter between 0.98 and 1 in. (25 and 25.4 mm), an ultimate strength of 65 ksi (450 MPa), and a yield characteristic strength of 51 ksi (350 MPa). The anchors were cast into the concrete specimens in a single cast. Wood formworks were used as a support for the anchors during the casting process so that they could easily be positioned at various embedment depths.

In the first set of the experiments, a single nominal embedment depth of 0.98 in. (25 mm), corresponding to a value of $d/c = 1$, was tested. This was necessary to complete the experimental data available in Piccinin et al. (2010), in which only $d/c = 2$ was thoroughly investigated.

In the second set, three different nominal embedment depths were used: 0.71, 1.97, and 2.7 in. (18, 50, and 69 mm). These values were chosen to obtain values of d/c equal to 0.75, 2, and 2.75, respectively. The smallest embedment depth was tested to determine the limit of applicability of a continuum mechanics approach.

Owing to the vibrating process and settlements during curing, the embedment depths at the time of the tests were slightly different from the nominal values, as listed in Table 2. Four anchors were placed on the four corners of each concrete specimen according to specifications spelled out in ACI 318 Appendix D (ACI 2008) and to avoid edge effects or undesired modes of failure (i.e., concrete blow out).

The tests were displacement controlled, and the relative displacements between the anchors and the upper surface of the concrete blocks were monitored by two LVDTs [±0.2 in. (±5 mm)] symmetrically positioned at a distance of 10.4 in. (264.2 mm) for short embedments and 15.2 in. (385 mm) for larger embedments. In all cases, the data (load and displacement) were acquired with an acquisition system.

The effect of confinement was simulated by applying biaxial compression along the sides of the concrete specimens in the directions orthogonal to the axis of the anchor. As shown in Fig. 5, the compression was applied by means of horizontally oriented hydraulic jacks inserted in a specially built reaction frame.

The steel beams used to build the reaction frame were tied together in the two plane directions by using six special Dywidag tying bars. On the two sides of the specimens that were subjected to the forces of the hydraulic jacks, two additional steel beams were used to uniformly distribute the horizontal pressure. The opposite sides of the specimens were loaded by contrast through the reaction

Table 1. Material Properties

Material	Property	Part I value [ksi (MPa)]	Part II value [ksi (MPa)]
Concrete	Cylinder strength, 28 days	4.73 (32.59)	3.36 (23.17)
	Cubic strength, 28 days	5.26 (36.30)	4.05 (27.91)
	Cylinder strength, 21 days	3.90 (26.90)	NA
	Cubic strength, 21 days	4.70 (32.40)	NA
	Tensile strength, f_t	0.42 (2.88)	0.41 (2.84)
	Young's modulus	3,408 (23,500)	3,300 (22,750)
Steel	Yield strength, 0.2% offset, f_y	51 (350)	51 (350)
	Ultimate strength, f_u	65 (450)	65 (450)

J. Eng. Mech. 2012.138:877-887.

Table 2. Experimental Investigation Details and Parameters

Part	Test	Nominal embedment length [in. (mm)]	Effective embedment length [in. (mm)]	Maximum confinement [kip (kN)]	Confining pressure σ_c [ksi (MPa)]
I	1	0.98 (25)	0.93 (24)	0 (0)	0 (0)
	2	0.98 (25)	0.97 (25)	0 (0)	0 (0)
	3	0.98 (25)	0.96 (24)	0 (0)	0 (0)
	4	0.98 (25)	0.91 (23)	0 (0)	0 (0)
	5	0.98 (25)	1.07 (27)	62 (276)	0.20 (1.34)
	6	0.98 (25)	1.03 (26)	62 (276)	0.20 (1.34)
	7	0.98 (25)	1.23 (31)	62 (276)	0.20 (1.34)
	8	0.98 (25)	1.06 (27)	89 (400)	0.29 (2.02)
	9	0.98 (25)	1.03 (26)	90 (400)	0.29 (2.02)
	10	0.98 (25)	0.98 (25)	121 (538)	0.39 (2.69)
	11	0.98 (25)	1.04 (26)	121 (538)	0.39 (2.69)
	12	0.98 (25)	0.94 (24)	121 (538)	0.39 (2.69)
II	1	0.71 (18)	0.83 (21)	0 (0)	0 (0)
	2	0.71 (18)	0.87 (22)	0 (0)	0 (0)
	3	0.71 (18)	0.77 (20)	0 (0)	0 (0)
	4	0.71 (18)	0.75 (19)	52 (232)	0.17 (1.16)
	5	0.71 (18)	0.97 (25)	52 (232)	0.17 (1.16)
	6	0.71 (18)	0.69 (18)	52 (232)	0.17 (1.16)
	7	0.71 (18)	0.66 (17)	52 (232)	0.17 (1.16)
	8	0.71 (18)	0.68 (17)	78 (347)	0.25 (1.74)
	9	0.71 (18)	0.75 (19)	78 (347)	0.25 (1.74)
	10	0.71 (18)	0.69 (18)	78 (347)	0.25 (1.74)
	11	0.71 (18)	0.68 (17)	78 (347)	0.25 (1.74)
	12	0.71 (18)	0.82 (21)	104 (463)	0.34 (2.32)
	13	0.71 (18)	0.82 (21)	104 (463)	0.34 (2.32)
	14	0.71 (18)	0.69 (18)	104 (463)	0.34 (2.32)
	15	0.71 (18)	0.71 (18)	156 (695)	0.50 (3.47)
	16	0.71 (18)	0.72 (18)	156 (695)	0.50 (3.47)
	17	1.97 (50)	1.80 (46)	0 (0)	0 (0)
	18	1.97 (50)	2.03 (52)	0 (0)	0 (0)
	19	1.97 (50)	2.00 (51)	0 (0)	0 (0)
	20	1.97 (50)	1.96 (50)	52 (232)	0.17 (1.16)
	21	1.97 (50)	2.06 (52)	52 (232)	0.17 (1.16)
	22	1.97 (50)	1.95 (50)	78 (347)	0.25 (1.74)
	23	1.97 (50)	1.89 (48)	78 (347)	0.25 (1.74)
	24	1.97 (50)	1.83 (46)	78 (347)	0.25 (1.74)
	25	1.97 (50)	2.29 (58)	104 (463)	0.34 (2.32)
	26	1.97 (50)	1.93 (49)	104 (463)	0.34 (2.32)
	27	1.97 (50)	2.27 (58)	104 (463)	0.34 (2.32)
	28	1.97 (50)	2.01 (51)	104 (463)	0.34 (2.32)
	29	1.97 (50)	1.90 (48)	156 (695)	0.50 (3.47)
	30	1.97 (50)	1.82 (46)	156 (695)	0.50 (3.47)
	31	1.97 (50)	2.04 (52)	156 (695)	0.50 (3.47)
	32	1.97 (50)	1.80 (46)	156 (695)	0.50 (3.47)
	33	2.70 (69)	2.93 (74)	0 (0)	0 (0)
	34	2.70 (69)	2.83 (72)	0 (0)	0 (0)
	35	2.70 (69)	2.83 (72)	52 (232)	0.17 (1.16)
	36	2.70 (69)	2.60 (66)	52 (232)	0.17 (1.16)
	37	2.70 (69)	2.62 (67)	78 (347)	0.25 (1.74)
	38	2.70 (69)	2.60 (66)	78 (347)	0.25 (1.74)
	39	2.70 (69)	2.62 (67)	78 (347)	0.25 (1.74)
	40	2.70 (69)	2.62 (67)	104 (463)	0.34 (2.32)

frame. To allow for a more uniform load distribution, a 0.4 in. [10 mm] layer of rubber band was positioned between the specimens and the frame. The pullout tests were first performed in unconfined concrete ($\lambda = 0$) for each value of embedment. Biaxial compression was subsequently considered. In the first part of the experiments, the tests in confined concrete were performed using values of λ in the range 0.47 to 0.94, whereas in the second part, values of λ equal to 0.41, 0.61, 0.82, and 1.22 were applied (details of the amount of force and relative stress applied to each specimen are shown in Table 2). The applied compression was constantly monitored before and after each pullout test with standard manometers.

In addition to the ultimate pullout forces and load-displacement curves, the shapes of the failure surfaces were also measured. For shallow anchors ($d/c = 1$), a very accurate observation of the crack profiles was made possible by a laser scanning machine. In this case, 3D crack profiles were obtained. By elaborating the available data, two-dimensional crack envelope profiles were then extrapolated. Because of the limited range of action of the scanning machine [about 1 in. (25.4 mm)], crack profiles for anchors with embedment depth $d/c = 2$ were reconstructed by visual inspection.

Results

Pullout Capacity

The experimentally measured normalized data for unstressed and prestressed concrete, together with the calibrated LEFM and nonlinear fracture mechanics (NLFM) numerical results, are shown in Figs. 6 and 7. The experimental ultimate capacities were nondimensionalized using the measured indirect tensile strengths of the materials and the effective embedment depths (Tables 1 and 2). Remarkably, the linear dependence on prestress predicted by the numerical models was consistent with the experimental results. In all cases in which $d/c \geq 1$, with respect to the unconfined case ($\lambda = 0$), an increase in capacity of about 12–15% was associated with a value of $\lambda \approx 1$. When $d/c = 0.75$, the experimental results presented larger scatter and the effects of prestress were not beneficial. It is noted that for the limit case where $d/c = 1$ and $\lambda \approx 1$ [Fig. 6(a)], a clear increase in capacity was not observed. A comparison between the LEFM model's predictions and the experimental results can be achieved by determining a reference value of β.

In Fig. 6(b), the results obtained from Piccinin et al. (2010) for $d/c = 2$ can be calibrated by using a reference value of $\beta \approx 0.6$, which corresponds to a value of fracture toughness for concrete equal to $K_{IC} \approx 0.755 \text{ ksi} \cdot \sqrt{\text{in.}}$ that is well within the range of typical values for concrete (between 0.18 and 1.26 $\text{ksi} \cdot \sqrt{\text{in.}}$). In Fig. 6(a), having decided to arbitrarily define L as the embedment depth, d, the experimental data are compared with the LEFM prediction associated with $\beta = 0.3$.

Similarly, in Fig. 7(c), the experimental results for $d/c = 2.75$ can be calibrated by using a value of $\beta \approx 1.13$, which corresponds to a value of fracture toughness $K_{IC} \approx 0.65 \text{ ksi} \cdot \sqrt{\text{in.}}$ for concrete. Remarkably, the behavior at $d/c = 2$ is also very well represented. On the other hand, for the corresponding value of $\beta \approx 0.31$ at $d/c = 0.75$, LEFM can only provide an upper bound to the experimental evidence.

Results from the NLFM simulations are also shown in Figs. 6 and 7. The traction-separation law used in this investigation is given by

Fig. 5. Built-in frame for the application of compressive prestress using hydraulic jacks

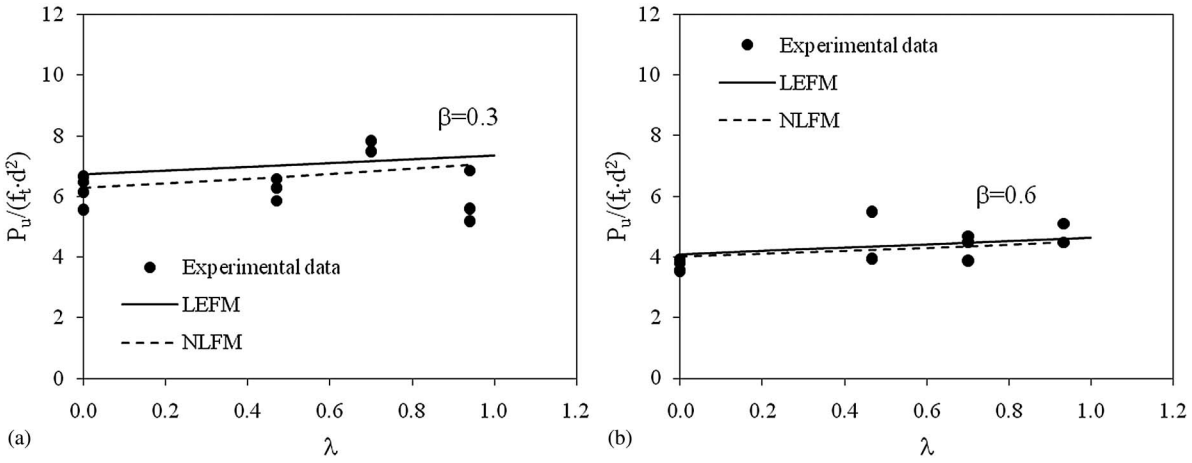

Fig. 6. Pullout load as a function of prestress and LEFM and NLFM calibration: (a) $d/c = 1$ (first set of experiments); (b) $d/c = 2$ (Piccinin et al. 2010)

$$\sigma = f_t \cdot \left(1 - \frac{\text{COD}}{\text{COD}_c}\right) \tag{5}$$

where f_t = indirect tensile strength of the material, COD = crack opening displacement, and COD_c = critical COD. The area under the curve defined by Eq. (5) is defined as the cohesive fracture energy G_f.

In each experimental set, the data obtained from the larger embedment depth investigated, $d/c = 2$ [Fig. 6(b)], and $d/c = 2.75$ [Fig. 7(c)], was used to calibrate the nonlinear fracture mechanics model, producing $G_f = 0.2$ lb/in. (35 N/m) and 0.15 lb/in. (27 N/m), respectively. The characteristic length of the fracture process zone is defined as (Shah et al. 1995)

$$l_{\text{ch}} = \frac{E \cdot G_f}{f_t^2} \tag{6}$$

For the current study, $l_{\text{ch}} \approx 4$ in. for the first set of experiments [which lies within the 4-in. (100-mm) to 16-in. (400-mm) range typical of concrete materials], whereas $l_{\text{ch}} \approx 3$ in. for the second set.

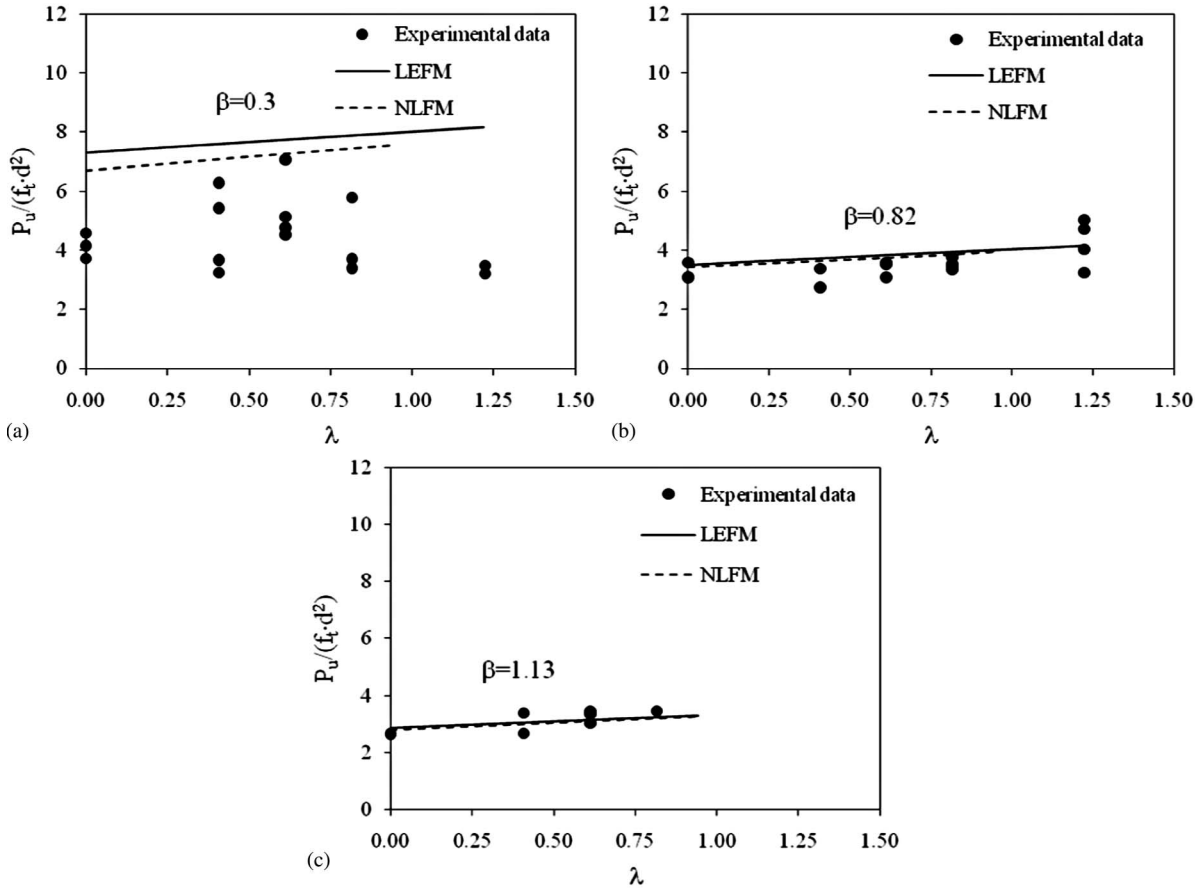

Fig. 7. Second set of experiments with pullout load as a function of prestress and LEFM and NLFM calibration: (a) $d/c = 0.75$; (b) $d/c = 2$; (c) $d/c = 2.75$

It is noted that the aforementioned values of the fracture energies are relatively low compared with the values available in the literature. CEB (1997), for example, recommended values of G_f of about 60 or 70 N/m for these types of concrete and aggregate sizes. However, the suggestion addresses concretes in which the water/cement ratio is around 0.3–0.4 and in which the cohesive law is usually specified as a softening bilinear function. In this case, the total fracture energy, G_f, is composed of an initial linear contribution that controls the peak load and a tail that quantifies the postpeak behavior. As indicated by the fact that high water/cement ratios provide lower values of G_f (Wittmann et al. 1987) and that only the linear contribution of the total fracture energy was calibrated to capture the experimental behavior, it is not surprising that relatively low values of G_f were determined.

It is clear that LEFM and NLFM provided identical and reasonable predictions for all the embedment depths investigated, except for $d/c = 0.75$. For this very shallow length scale, it seems that a deterministic continuum-based model cannot capture the experimental behavior. This can be alternatively shown for the unstressed case ($\lambda = 0$). Fig. 8 shows the experimental results in comparison with the existing design formulas. In a log-scale plot, the pullout loads are normalized with respect to the area of a circle of radius equal to the embedment depth, d. When compared with the numerical predictions, the CCD formula provided identical predictions for relatively large embedment depths and was a lower (conservative) bound for shallow anchors. Fig. 8(b) shows that the behavior of anchors embedded at $d/c = 0.75$ is unpredictable. This is true from a quantitative (the results are between the LEFM and the plasticity-based predictions) and qualitative (the results show, in fact, a significant scatter) point of view. Further support to these observations is provided subsequently, where crack profiles from the experimental investigation are shown.

Load versus Displacement Behavior

The effects of prestress on ductility were quantified using the work of fracture (WOF), defined as the area under the normalized force-displacement curve. Results from the NLFM simulations are shown in Fig. 9. LEFM results, as reported in Piccinin et al. (2010), had proven to be identical. For a value of $G_f = 0.2$ lb/in. (35 N/m), when a confining (compressive) prestress was applied, the energy dissipated in the postpeak increased. This increase was the result of the significant increase in the length of crack propagation. It is noted that the curves shown are truncated when the load in the postpeak range is about half the peak value. Numerical instabilities arise when the stress free portion of the fictitious crack is significantly larger than the cohesive counterpart.

It is noted that in the experiments, the displacement was measured by two LVDTs positioned symmetrically with respect to the axis of the anchor, whereas in the numerical model the displacement was defined as the crack opening displacement of the infinitely small slit representing the bolt (Fig. 2, Δ).

Even though qualitative—and based on different definitions of the load-point displacement, Δ—the significant postpeak ductile behavior of the system and the increase in capacity and ductility with the applied compressive stress are shown in Fig. 10. Clearly, and as previously observed, Fig. 9 illustrates that the NLFM predictions only provide a lower bound solution to the experimental evidence. The writers have not yet determined why there are such

J. Eng. Mech. 2012.138:877-887.

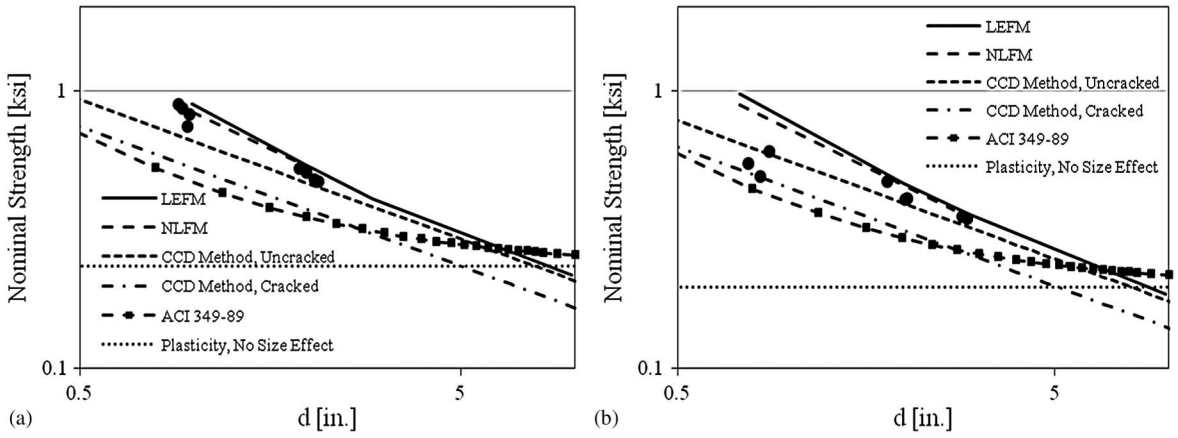

Fig. 8. Log-log plot of nominal pullout strength as a function of the embedment depth for the embedment depths investigated in which $\lambda = 0$ and (a) $d/c = 1$ (first set of experiments) and $d/c = 2$ (Piccinin et al. 2010) and (b) $d/c = 0.75$, $d/c = 2$, and $d/c = 2.75$; experimental data represented by discrete points

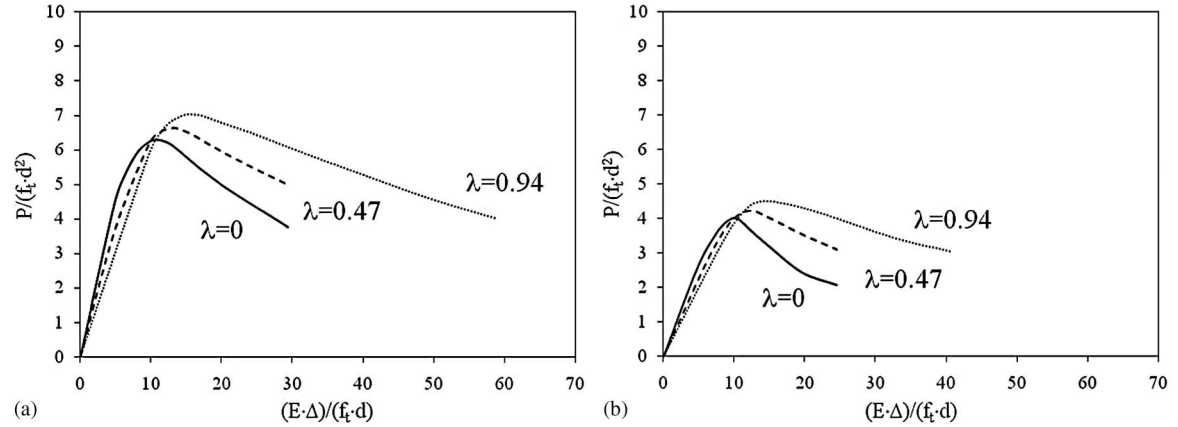

Fig. 9. Numerical load-displacement curves for (a) $d/c = 1$ and (b) $d/c = 2$ and various levels of prestress

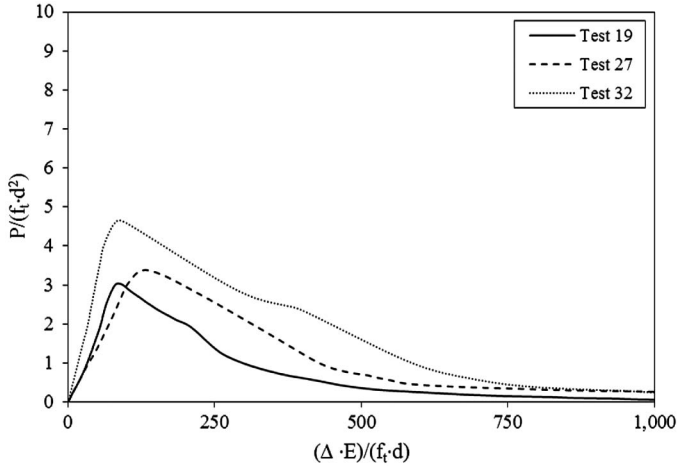

Fig. 10. Experimental normalized load-displacement curves for $d/c = 2$ and various levels of prestress ($\lambda = 0$, 0.82, and 1.22)

discrepancies between the experimental load-displacement curves and those predicted by the idealized model of the anchor. The sources of the discrepancy may be a result of the following: (1) the concrete near the top surface of the anchor's head may have experienced crushing; (2) the physical anchor contains a stem, which could lead to a less stiff response than the response predicted by the idealized infinitely thin slit anchor geometry; and/or (3) the computational model did not take into account slippage, friction, and other displacement contributions that may have occurred during the pullout tests.

Crack Profiles

Crack profiles from the experimental studies and LEFM investigations are shown in Fig. 11 for $d/c = 1$ (laser machine readings) and in Fig. 12 for $d/c = 2$ (visual inspection), for several values of λ. First, it is clearly shown that the propagating crack front steers toward the direction of application of the compressive stresses (e.g., the horizontal direction, orthogonal to the axis of the anchor). This was true for all the embedment depths investigated and was enhanced when large compressions were applied (Piccinin et al. 2010). Second, it appears that the experiments do not differ significantly from the numerical LEFM results. Considering the simplicity of the finite-element model and the fact that inhomogeneities and aggregates can give rise to very tortuous crack paths, LEFM does a good job of predicting the crack paths. It is noted, more importantly, that these results support the method adopted to carry out the NLFM numerical simulations, which were based on the use of cohesive elements along LEFM predefined crack paths.

Experimental observations of the crack profiles and the cone sizes for anchors embedded at $d/c = 0.75$ were also completed

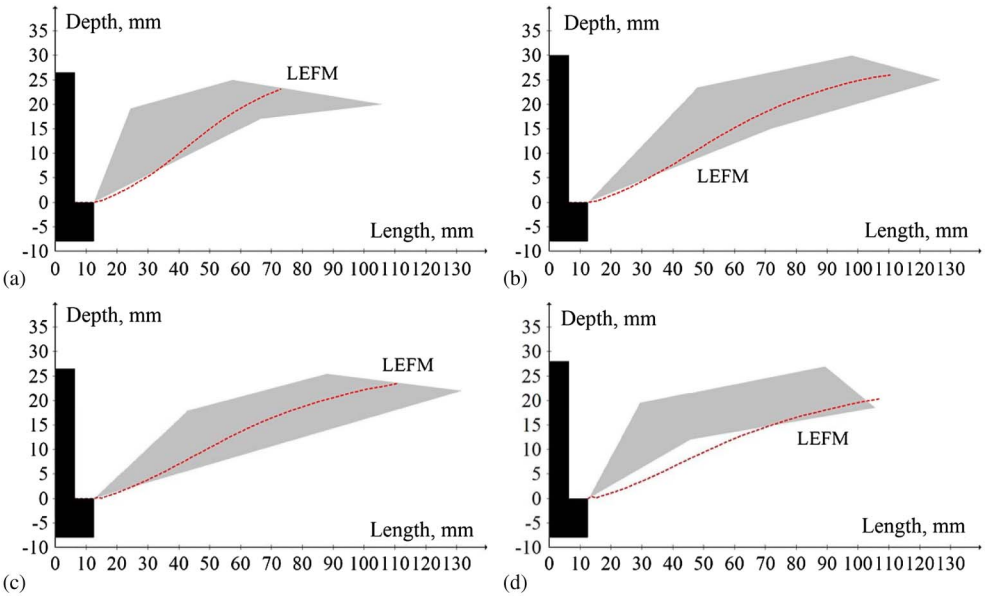

Fig. 11. Comparison of crack profiles from the experiments (shaded gray area/envelope) and LEFM simulations (dashed line) in which $d/c = 1$ and (a) $\lambda = 0$; (b) $\lambda = 0.47$; (c) $\lambda = 0.7$; and (d) $\lambda = 0.94$

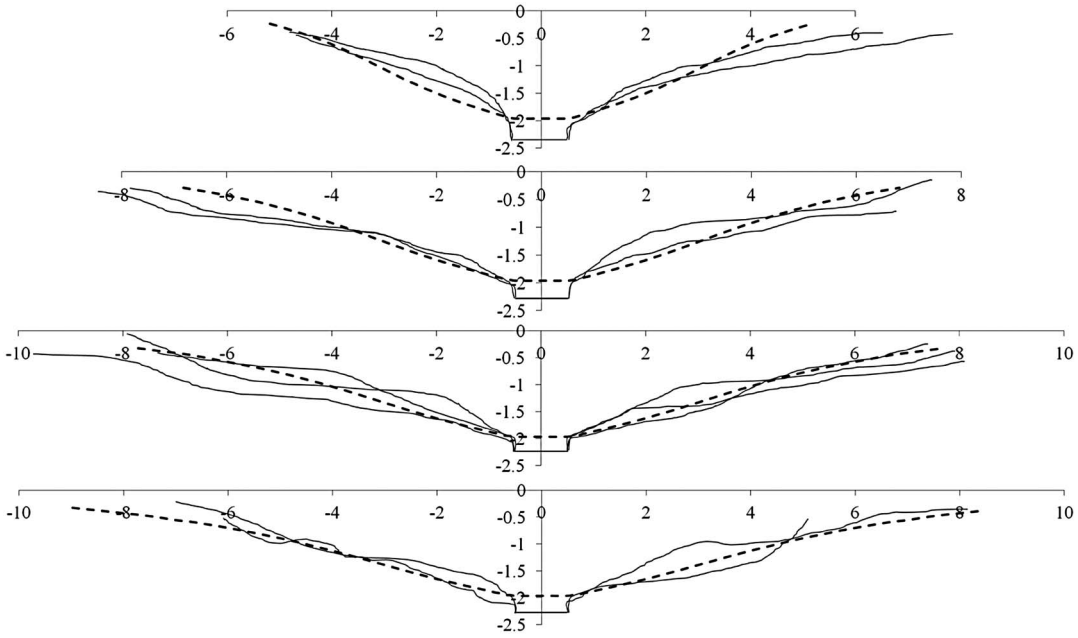

Fig. 12. Comparison between LEFM predictions (dashed lines) and experimental crack propagation patterns (from top to bottom); $d/c = 2$ and $\lambda = 0$, 0.41, 0.61, and 0.82

(data not shown). For such small embedments, the size of the aggregate was comparable to the characteristic dimensions of the experiments and the models. The experiments for these cases resulted in the pulling out of the anchors as a result of discrete cracks propagating at the interface between the matrix and the aggregate and remaining unchanged for the unstressed and stressed cases. Thus, the cracks in the experiments cannot possibly take on the paths predicted by the mixed mode crack propagation theory used in the homogeneous material model. For example, if the aggregate is slightly to the left of the anchor tip shown in the schematic of the model (Fig. 2), propagation along the interface would be almost vertical and typical of pullout of a cohesionless granular material. This result supports the conclusion that the size effect is the strongest possible down to such small embedments and that a continuum-based theory cannot be applied to cases where the length scale involved is comparable to the dimension of the largest aggregate.

Design Formula

The present investigation shows that for values of $0 \leq \lambda \leq 1.25$ and $0 < \beta \leq 10$, the design formula based on LEFM concepts and

J. Eng. Mech. 2012.138:877-887.

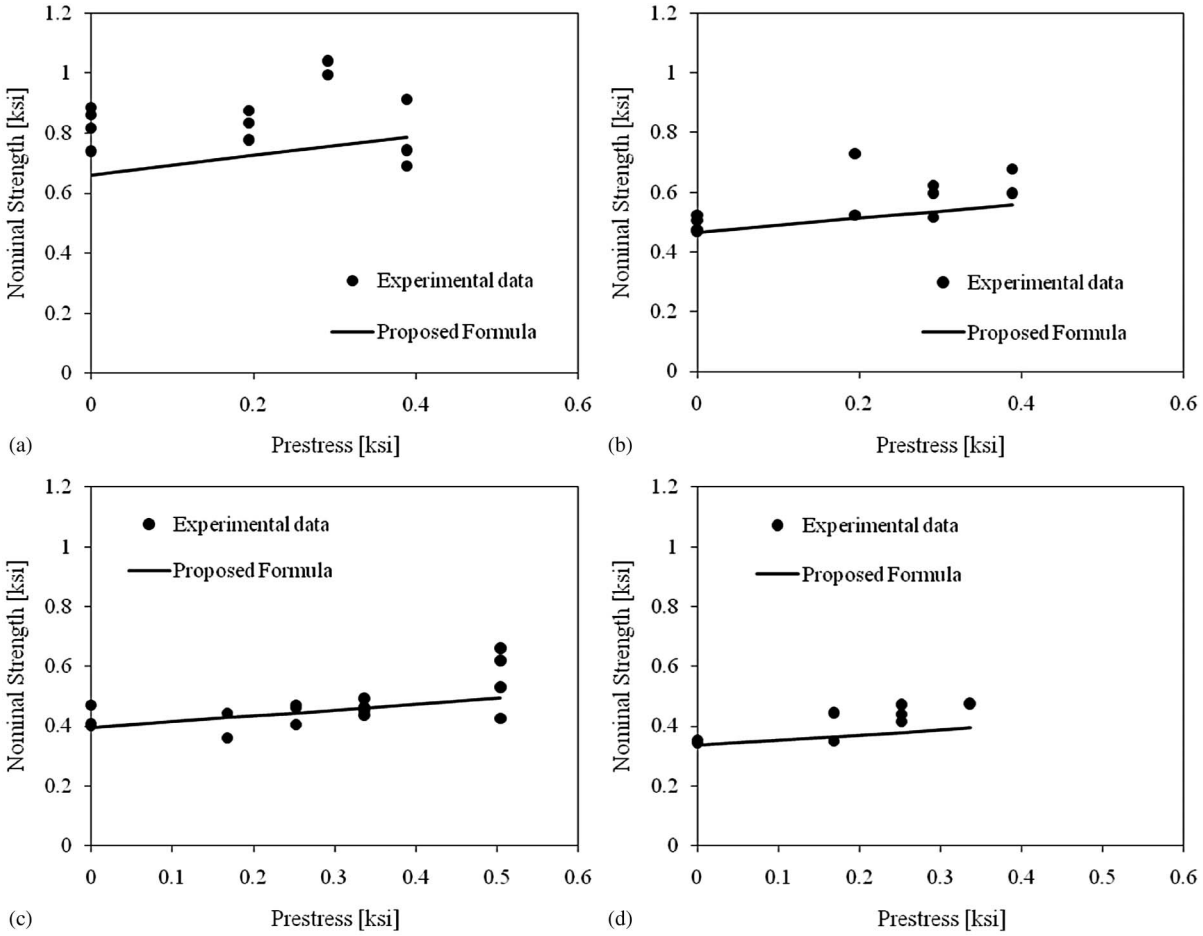

Fig. 13. Comparison of the experiments and proposed design [Eq. (8)]: (a) $d/c = 1$ and (b) $d/c = 2$ (first set of experiments); (c) $d/c = 2$ and (d) $d/c = 2.75$ (second set of experiments)

proposed in Piccinin et al. (2010) still holds. This formula can be expressed as

$$\frac{P_u}{f_t d^2} = \frac{3.15}{\sqrt{\beta}} + 0.53\lambda \tag{7}$$

By combining Eqs. (1) and (7), for $0 \le \lambda \le 1.2$ and only for $d/c \ge 1$, an accurate fit of the numerical predictions and the experimental evidence leads to the following, more practical, design formula:

$$P_u = (k_{nc} + 0.015 \cdot \sigma_c) \cdot \sqrt{f'_c} \cdot d^{3/2} \tag{8}$$

where $k_{nc} = 30$ (uncracked concrete condition), P_u is expressed in lb, and σ_c and f'_c are expressed in psi. A comparison between the experimental results and the proposed formula is shown in Fig. 13, in which the pullout loads are normalized with respect to the area of a circle of radius equal to the embedment depth d.

Being based on Eq. (1), the proposed formula for the capacity of headed anchors in a compressively stressed concrete matrix represents a lower bound for shallow anchors. However, it represents a sufficiently accurate and conservative fit for all the other embedment depths.

Conclusions

The results from the present investigations show that the capacity of headed anchors is increased when compressive prestress is applied to the concrete matrix. As a consequence, a design formula validated through numerical and experimental investigations is proposed. However, it is recommended that further studies be carried out before its application.

It is recognized that LEFM and NLFM provide very similar results and are both valid for scale lengths as small as $d/c = 1$, which have never been investigated before. This provides valuable insights into the behavior of headed anchors, and it is concluded that the pullout failure is a problem governed by the maximum possible concrete's size effect and that no transition between strength-based theory and LEFM is expected. For the limit case in which $d/c = 1$ and $\lambda \approx 1$, the increase in capacity predicted by the numerical models is not completely corroborated by the experimental evidence. Further investigation is required to enlighten this case. For embedments $d/c < 1$, that is, for scale lengths smaller than the maximum aggregate size, this investigation shows that the pullout problem cannot be solved by applying a deterministic continuum theory.

Acknowledgments

The experimental part of this research was carried out with the support of the Yucatan Decima concrete precast plant and its technical staff. The staff of the Laboratorio Prove Materiali of the Politecnico di Milano is also gratefully thanked. The writers express their gratitude to Professor L. Biolzi, Professor G. Rosati, and D. Spinelli for their valuable advice, constant encouragement,

and tireless dedication, and Dr. P. Wawrzynek and Professor A. Ingraffea from Cornell University for their support in understanding and using their software.

References

American Concrete Institute (ACI). (1989). "Code requirements for nuclear safety." Appendix B, *ACI 349.1R*, ACI, Detroit.

American Concrete Institute (ACI). (2006). "Code requirements for nuclear safety related concrete structures and commentary." Appendix D, *ACI 349-06 and ACI 349R-06*, ACI, Farmington Hills, MI.

American Concrete Institute (ACI). (2008). "Building code requirements for structural concrete and Commentary." Appendix D, *ACI 318-08 and ACI 318R-08*, ACI, Farmington Hills, MI.

Ballarini, R., Keer, L. M., and Shah, S. P. (1987). "An analytical model for the pull-out of rigid anchors." *Int. J. Fract.*, 33(2), 75–94.

Ballarini, R., Shah, S. P., and Keer, L. M. (1986). "Failure characteristics of short anchor bolts embedded in a brittle material." *Proc. R. Soc. London, Ser. A*, 404(1826), 35–54.

Baran, E., Schultz, A. E., and French, C. E. (2006). "Tension tests on cast-in-place inserts: The influence of reinforcement and prestress." *PCI J.*, 51(5), 88–108.

Bažant, Z. P., and Planas, J. (1998). *Fracture and size effect in concrete and other quasibrittle materials*, CRC, Boca Raton, FL.

Bažant, Z. P., and Sener, S. (1988). "Size effect in pullout tests." *ACI Mater. J.*, 85(5), 347–351.

Bittencourt, T. N., Ingraffea, A. R., and Llorca, J. (1992). "Simulation of arbitrary, cohesive crack propagation." *Fracture mechanics of concrete structures*, Z. P. Bažant, ed., Elsevier Applied Science, London, 339–350.

Cherepanov, G. P. (1979). *Mechanics of brittle fracture*, McGraw-Hill, New York.

Comité Euro-International du Béton (CEB). (1997). *Design of fastenings in concrete: Design guide*, Thomas Telford, London.

Cornell Fracture Group. (1997). *FRANC2D*, Cornell Fracture Group, Cornell Univ., Ithaca, NY. ⟨http://www.cfg.cornell.edu/software/franc2d_casca.htm⟩ (Jun. 2008).

Elfgren, L., and Ohlsson, U. (1992). "Anchor bolts modeled with fracture mechanics." *Application of fracture mechanics to reinforced concrete*, A. Carpinteri, ed., Elsevier Applied Science, London, 267–283.

Eligehausen, R., and Ozbolt, J. (1990). "Size effect in anchorage behavior." *Fracture behavior and design of materials and structures*, D. Firrao, ed., Vol. 2, Engineering Materials Advisory Services, Ltd., Warley, West Midlands, UK, 721–727.

Eligehausen, R., and Sawade, G. (1989). "Analysis of anchorage behaviour (literature review)." *Fracture mechanics of concrete structures: From theory to applications*, L. Elfgren, ed., Chapman & Hall, London, 263–280

Fuchs, W., Eligehausen, R., and Breen, J. E. (1995). "Concrete capacity design (CCD) approach for fastening to concrete." *ACI Struct. J.*, 92(1), 73–94.

Hellier, A. K., Sansalone, M., Ingraffea, A. R., Carino, N. J., and Stone, W. C. (1987). "Finite element analysis of the pull-out test using a nonlinear discrete cracking approach." *Cem., Concr., Aggregates*, 9(1), 20–29.

Ingraffea, A. R., Linsbauer, H., and Rossmanith, H. (1989). "Computer simulation of cracking in large arch dam—downstream side cracking." *Fracture of concrete and rock*, S. P. Shah and S. E. Swartz, eds., Springer, New York, 334–342.

Ingraffea, A. R., and Saouma, V. (1984). "Numerical modeling of fracture propagation in reinforced and plain concrete." *Fracture mechanics of concrete: Structural application and numerical calculation*, G. C. Shih and A. Di Tommasi, eds., Martinus Nijhoff, Dordrecht, Netherlands, 171–225.

Jensen, B. C., and Braestrup, H. W. (1976). *Lok-tests determine the compressive strength of concrete*, No. 2, Nordisk Betong, Stockholm, Sweden, 9–11.

Ottosen, N. S.. (1981). "Nonlinear finite element analysis of pull-out test." *J. Struct. Div.*, 107(4), 591–603.

Ozbolt, J., Eligehausen, R., and Reinhardt, H. W. (1999). "Size effect on the concrete cone pull-out load." *Int. J. Fract.*, 95(1-4), 391–404.

Piccinin, R. (2011). "Effects of compressive and tensile fields on the load carrying capacity of headed anchors." Ph.D. dissertation, Univ. of Minnesota, Minneapolis.

Piccinin, R., Ballarini, R., and Cattaneo, S. (2010). "Linear elastic fracture mechanics pullout analyses of headed anchors in stressed concrete." *J. Eng. Mech.*, 136(6), 761–768.

Pivonka, P., Lackner, R., and Mang, H. A. (2004). "Concrete subjected to triaxial stress states: Application to pull-out analyses." *J. Eng. Mech.*, 130(12), 1486–1498.

Reinhardt, H. W. (1981). "Masstabsein uss bei Schubversuchen im Licht der Bruchmechanik." *Beton- Stahlbetonbau*, 1, 19–21.

Shah, S. P., Swartz, S. E., Ouyang, C. (1995). *Fracture mechanics of concrete: applications of fracture mechanics to concrete, rock, and other quasi-brittle materials*, Wiley, New York.

Vogel, A., and Ballarini, R. (1999). "Ultimate load capacities of plane and axisymmetric headed anchors." *J. Eng. Mech.*, 125(11), 1276–1279.

Wawrzynek, P. A., and Ingraffea, A. R. (1987). "Interactive finite element analysis of fracture processes: An integrated approach." *Theor. Appl. Fract. Mech.*, 8(2), 137–150.

Wittmann, F. H., Roelfstra, P. E., and Mihashi, H. (1987). "Influence of age of loading, water-cement ratio and rate of loading on fracture energy of concrete." *Mater. Struct.*, 20(2), 103–110.

Xie, M., and Gerstle, W. (1995). "Energy-based cohesive crack propagation modeling." *J. Eng. Mech.*, 121(12), 1349–1358.